

## **Salicylic acid induces the formation of supramolecular antimicrobial hydrogels from worm-like micelles**

Dongfang liu<sup>a,b\*</sup>, Liqin Huang<sup>a</sup>, Yu Jing<sup>a</sup>, Tingmei Huang<sup>a</sup>, Di Zhang<sup>a</sup>, Dong Jiang<sup>a</sup>, Yaxin Zhao<sup>c</sup>,  
Yuanyuan Zhang<sup>a\*</sup>

<sup>a</sup> Department of Chemistry, School of Science, Xihua University, Chengdu, P. R. China, 610039

<sup>b</sup> Oil & Gas Field Applied Chemistry Key Laboratory of Sichuan Province, Chengdu,  
P. R. China, 610500

<sup>c</sup> Chengdu Newsun Crop Science Company Limited, Pujiang, Chengdu, Sichuan, 611630

## **1. Materials and Methods**

### **1.1 Worm-like micelles and gel preparation LGS/CTAB**

First, accurately weigh 0.40 g of LGS solid powder and 0.8 g of CTAB powder. Place these powders into a beaker and add deionized water to bring the total mass to 40 g. After mixing thoroughly, immerse the beaker in a 60°C water bath until all powders dissolve completely, forming an LGS/CTAB wormlike micelle solution. Then, transfer the solution to a 25°C water bath for cooling and adjust the pH to 6 to promote the formation of the LGS/CTAB wormlike micelle structure.

First, weigh 0.40 g of LGS powder and an appropriate amount of SA, add them to a beaker, and supplement with deionized water to a total weight of 40 g. After thorough mixing, heat the mixture in a 60°C water bath until transparent. During this process, add 1 mol/L HCl to adjust the pH to 2.5. Subsequently, transfer the solution to a 25°C water bath for cooling and let it sit to form an LGS/SA supramolecular hydrogel. In this gelation process, the mass ratio of LGS to SA is 1:1, resulting in a hydrogel concentration of 1 wt%.

### **1.2 Aggregate Size and Zeta-potential Testing**

Particle size and zeta potential measurements are conducted at ambient temperature using a nano particle size and zeta potential analyzer (BeNano 180 Zeta, Dandong Biotek Instrument Co., Ltd.). For particle size analysis, the procedure involves transferring 1 milliliter of the sample into a glass cuvette, which is then placed in the measurement chamber. The instrument settings are adjusted as necessary, and the analysis is initiated to determine the particle size distribution of the sample.

For the zeta potential measurement, the sample is drawn into the capillary electrode and then inserted into the testing cell. The instrument settings are recalibrated as required, and the measurement of the sample's zeta potential is commenced.

### **1.3 Microstructure Testing**

Microstructure analysis was conducted using a polarizing microscope (CX40P, Ningbo Sunny Instrument Co., Ltd.). For the LGS/CTAB precipitation phase analysis, a droplet of the sample solution is placed on a glass slide with a pipette. The slide is

then positioned on the microscope stage, and the microscope is calibrated for optimal settings before starting the observation process.

For the preparation and observation of the LGS/SA hydrogel microstructure, mix LGS with SA in a 1:1 mass ratio at a concentration of 1 weight percent. Heat the solution to 60°C and adjust the pH as required. Using a collet dropper, place a drop of the sample solution onto the center of a clean glass slide. Gently cover with a coverslip and allow it to cool to room temperature for a sufficient period. Once cooled, transfer the slide to the sample stage of a polarizing microscope and adjust the instrument settings to achieve the best possible observation of the sample microstructure.

## **2. Results and discussion**

### **2.1 LGS/CTAB Precipitation Phase Analysis**

In the presence of a low concentration of CTAB (0.5 wt%), the LGS/CTAB system exhibited a limited range of precipitation, allowing for observation of its microstructure. Illustrated in Figure S1, under pH=5 and pH=2 conditions, the LGS/CTAB system appeared as a homogeneous opaque solution, with spherical aggregates observed in the microstructure. Notably, at pH=5, smaller and more uniformly dispersed aggregates were observed, while at pH=2, the aggregates appeared relatively larger, accompanied by the presence of textured structures, indicating fewer three-dimensional structures within the LGS/CTAB system. Conversely, at pH=4 and pH=3, the LGS/CTAB system exhibited white precipitation, with the microstructure revealing the aggregation of globular structures. Further aggregation of these globular aggregates reduced solubility, resulting in the observed white precipitation.

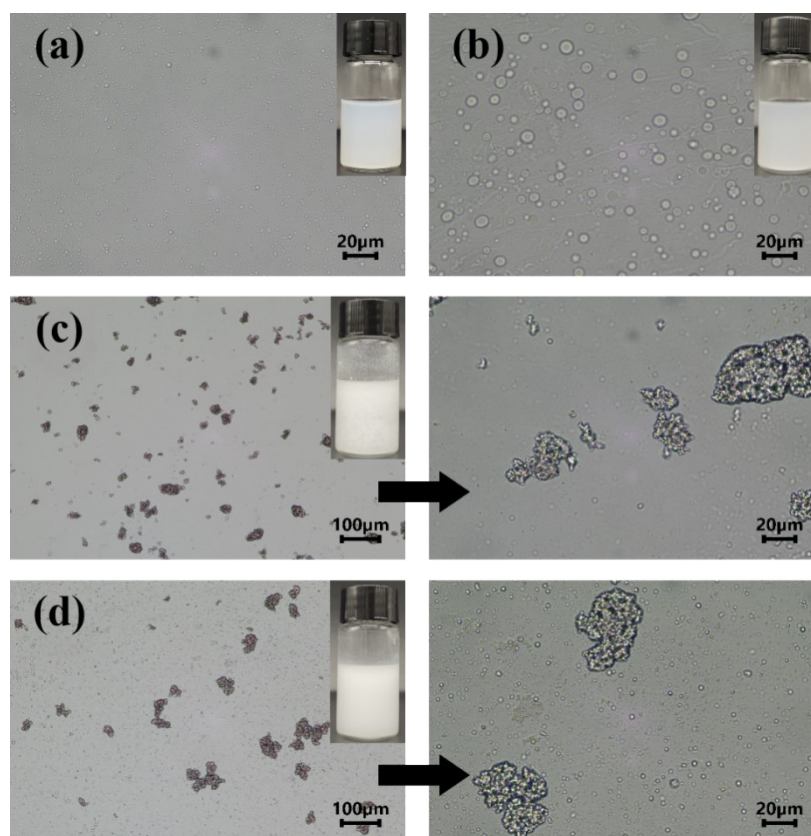


**Figure S1.** Microscopic diagram of the LGS/CTAB hybrid system at different pH conditions (a) pH=5 (b) pH=2 (c) pH=4 (d) pH=3

The LGS/CTAB hybrid system exhibited more spherical aggregates under pH=5 and pH=2 conditions, with their particle size and potential analyzed. Table S1 demonstrates that at pH=5, the aggregate potential is -42.66mV, attributed to LGS molecules providing a greater negative charge compared to the positive charge from CTAB, resulting in negatively charged aggregates. As pH decreases, the molecular state of LGS transitions from LGS<sub>1</sub> to LGA, leading to a sharp decrease in charge, while the pH-independent charged nature of CTAB maintains positively charged aggregates at pH=2, averaging 41.64 mV. Aggregate particle sizes align with microstructural observations, with notably smaller sizes observed at pH=5 compared to pH=2.

**Table S1.** Particle size and potential testing of LGS/CTAB hybrid system

pH	aggregate size (nm)	PDI	mean potential (mV)
5	161.59	0.337	-42.66
2	303.75	0.383	41.64

## 2.2 Preparation of LGS/CTAB WLMs

In a neutral environment, the mixed system of LGS and CTAB can form WMLs,

and the viscosity of the system increases sharply. As shown in Figure 2(a), when the concentration of LGS is fixed at 1 wt%, under the condition of a low-concentration CTAB (0.5 wt%), WLMs do not appear in the mixed system, and three different states are presented: a color-less transparent solution (Phase III), a homogeneous blue solution (Phase I), and a white precipitate (Phase V). Under the condition of  $\text{pH} \geq 6$ , the mixed solution of 1 wt% LGS and 0.5 wt% CTAB shows a color-less transparent state with almost no viscosity. The possible reason is that in an alkaline environment, LGS exists in the  $\text{LGS}_2$  state, which has strong hydrophilicity and self-assembles with CTAB to form a spherical micelle structure, resulting in almost no change in the viscosity of the system. As the pH decreases, the system transforms into a homogeneous blue dispersion system, yet there is still no change in viscosity. The possible reason is that there is an assembled structure between LGS and CTAB. The decrease in pH leads to the transformation of LGS into the  $\text{LGS}_1$  molecular state, which is conducive to the aggregation of LGS and CTAB molecules. At the same time, the aggregates carry certain charges, enabling them to disperse uniformly in water, presenting as a homogeneous dispersion system. With a further decrease in pH, the transformation of the LGS molecular state leads to a decrease in the charge of the LGS/CTAB aggregates, forming a larger aggregated structure. The solubility of the aggregates decreases, resulting in the formation of a precipitate. Under the condition of  $\text{pH} \leq 2$ , the precipitate gradually disappears. The reason is that the negative charge of the LGS molecules gradually disappears, and the aggregates exhibit the positive charge imparted by CTAB. The aggregates disperse uniformly again, presenting as a light - blue homogeneous dispersion system.

Concentration also affects the apparent morphology of the aggregates. When the concentration of CTAB increases to 1.25 wt%, under the condition of  $\text{pH} = 6$ , the viscosity of the LGS/CTAB solution increases sharply (Phase II), and LGS/CTAB WLMs are formed at this time. A new macroscopic phenomenon also appears in the system, namely a layered structure (Phase IV), with an assembly structure similar to micelles in the upper layer and an aqueous solution in the lower layer. The possible reason is that the concentration of CTAB is relatively low at this time, which is

insufficient to construct a complete WLMs network. When the concentration of CTAB is 2 wt%, under the condition of  $\text{pH} \leq 6$ , the LGS/CTAB system exhibits a complete WLMs phase. The LGS/CTAB mixed system under this concentration condition is subjected to rheological analysis to further verify the formation of the WLMs structure.

### 2.3 Standard curve of SA aqueous solution

The standard curve for SA was established using UV spectrophotometry, depicted in Figure S2 (a). Initially, the characteristic peaks of SA were identified within the range of 200~600 nm, with peaks observed at 230.5 nm and 296 nm. The peak at 296 nm was chosen as the standard for constructing the SA aqueous solution's standard curve, illustrated in Figure S2 (b). The equation for the SA standard curve is  $y=24.388x-0.01708$ , with a correlation coefficient of  $R^2=0.99807$ .

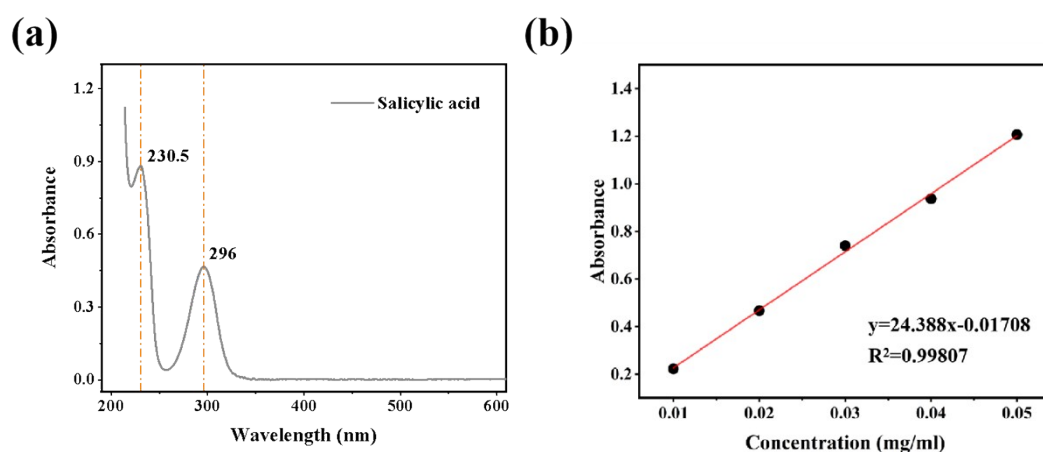


Figure S2. (a) SA uv-vis absorption spectrum (b) Standard SA curve

### 2.4 Formation of LGS/SA supramolecular hydrogel

Figure S3 (a) demonstrates that LGS and SA are capable of forming supramolecular hydrogels. At ambient temperature, SA exhibited superior water solubility compared to LGS, resulting in a turbid state when a mixed aqueous solution of 1 wt% LGS and 1 wt% SA was prepared. Upon heating to 60°C, both LGS and SA dissolved completely, rendering the solution transparent. pH adjustment during stirring induced a transition from a transparent solution to a homogeneous opaque sol state, and upon natural cooling to room temperature (25°C), LGS/SA gels were successfully formed.

To explore the impact of SA concentration on gel formation, LGS concentration

was held constant at 1 wt%, while SA concentration was varied to observe its influence on the gel state. As depicted in Figure S3 (b), Herein, "pcpn" is the abbreviation for "precipitation phenomenon," "gel + sol" refers to the coexistence of gel with water, and "gel" is the abbreviation for "gel phase." The addition of SA markedly affected gel formation. At an SA concentration of 0.5 wt%, the mixed solution ceased to exhibit a gel state at pH=3, transitioning instead to a mixed state of gel and solution. This phenomenon likely arises from SA's involvement in the network construction of the gel, where a portion of SA competes for hydrogen bonding sites on LGS molecules, thereby altering the gel structure. At an SA concentration of 0.5 wt%, the pH ranged from 3 to 2, with the mixed solution demonstrating coexistence of gel and solution. As SA concentration increased, gel formation occurred over a broader pH range. This can be attributed to the heightened participation of molecules in gel construction with increasing SA concentration, leading to a more comprehensive network structure.

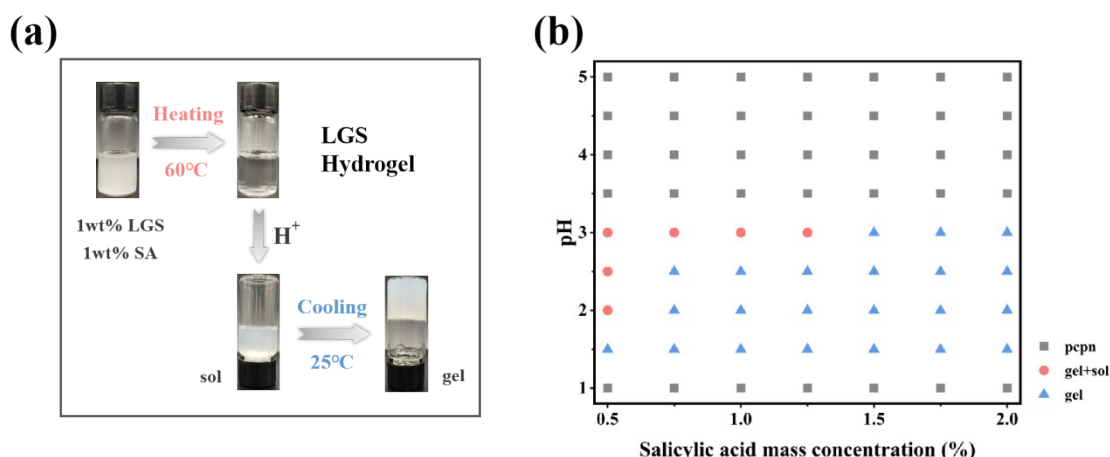


**Figure S3.** LGS/SA supramolecular hydrogel (a) preparation process (b) forming range diagram

Figure S4 illustrates the microstructure of the gel. In the mixed system containing 1 wt% LGS and 1 wt% SA, at pH=4, an abundance of precipitates with a fiber-like crystal structure is evident in the mixed solution. As pH decreases to 3, assembled structures appear in the solution, yet no gel forms. Within the pH range of 2.5 to 1.5, the mixed solution transitions into a gel state. At pH 2.5 to 1.5, the gel exhibits rod-like crystal structures, possibly due to the orderly arrangement of SA molecules. As pH further decreases, the gel state transforms into a precipitated state, with precipitation attributed to the assembled structures of LGS molecules attached to the rod-like

crystals.

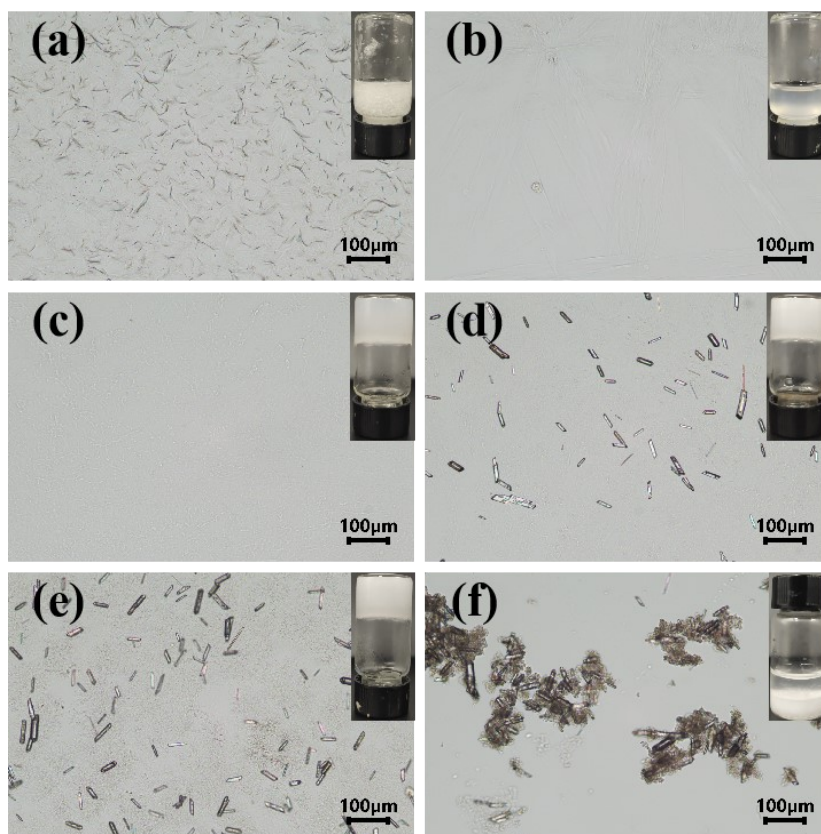


**Figure S4.** Microscopic diagram of LGS/SA mixed system at different pH conditions (a) pH=4 (b) pH=3 (c) pH=2.5 (d) pH=2 (e) pH=1.5 (f) pH=1

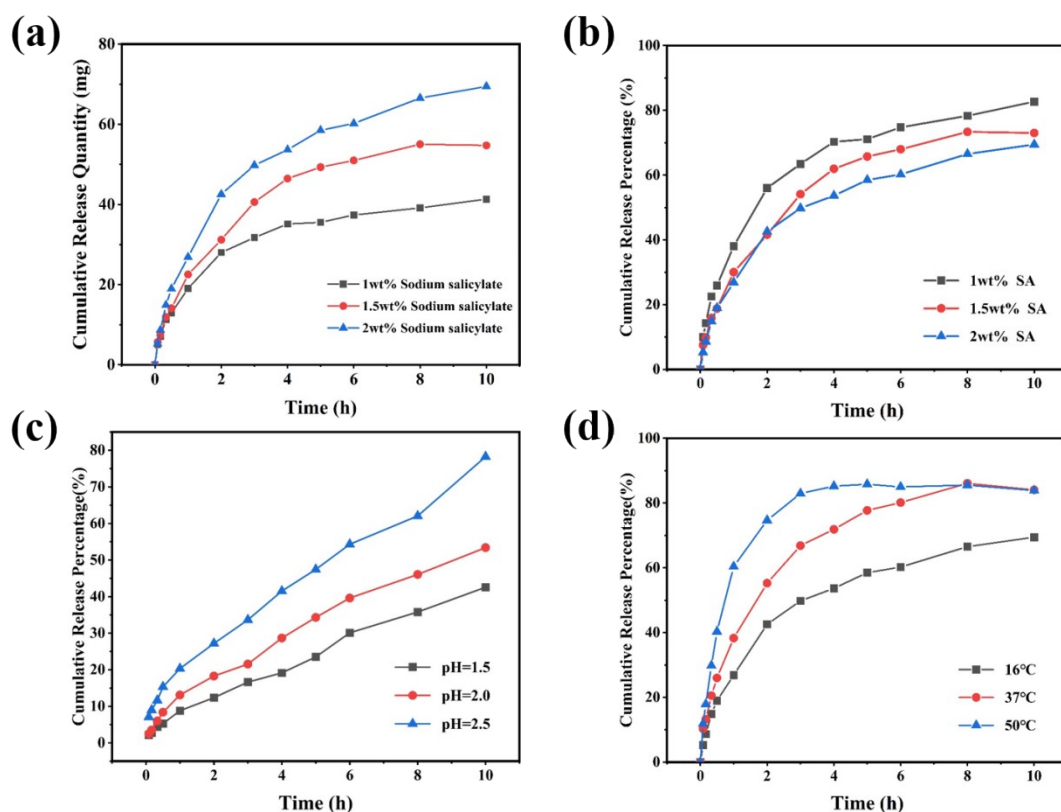
## 2.5 Effects of different conditions on the slow-release behavior of LGS/SA hydrogels

At room temperature, the influence of SA acid concentration on the drug release rate from LGS/SA hydrogels was examined. The hydrogels were immersed in a phosphate buffer solution, and drug release into the buffer was monitored at various time points using a UV spectrophotometer. Drug release was quantified based on a standard curve from the UV readings. Figures S5 (a) and (b) show an initial rapid drug release followed by a stabilization phase. Intriguingly, while a higher SA concentration increased the total drug released due to greater drug loading, it also resulted in a slower release rate. This apparent contradiction is likely due to SA's contribution to the hydrogel's denser three-dimensional network structure, which impedes drug release.

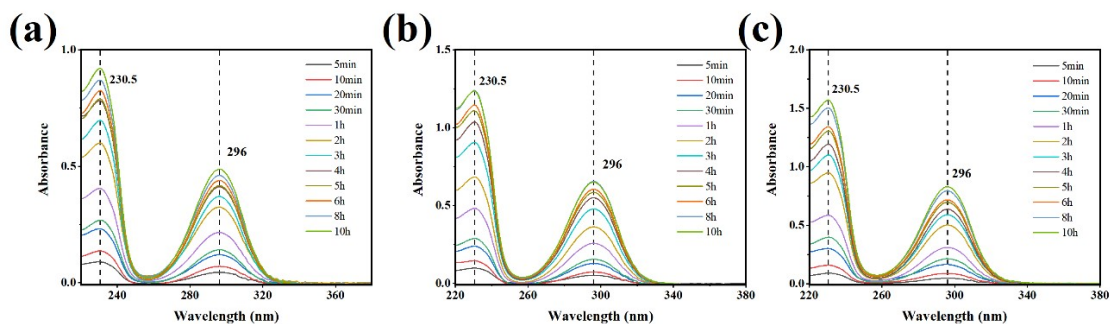
To study the impact of pH on the controlled release of the LGS/SA gel system, hydrogels were prepared at various pH levels with a constant SA concentration of 2 wt%. Afterward, these hydrogels were placed in a phosphate buffer solution (refer to

Figure S7). Drug release into the buffer was then measured using UV spectrophotometry over time, scanning wavelengths between 220 nm and 380 nm. The amount of drug released was determined using a standard curve from the UV data. Figure S5 (c) shows that the drug release rate is significantly affected by the pH, with higher pH values leading to increased drug release rates. This phenomenon occurs because a higher pH loosens the hydrogel's 3D network, enabling easier drug diffusion.

To assess the effect of temperature on the LGS/SA hydrogel's slow release, a hydrogel with 2 wt% SA at pH 2.5 was prepared and exposed to various temperatures in a phosphate buffer solution (Figure S8). Drug release into the buffer was measured using UV spectrophotometry over time. The results in Figure S5 (d) show that the drug release rate increases with temperature, stabilizing at 60% at room temperature and peaking at 80% at human body temperature. Higher temperatures also accelerate the time to release equilibrium.



**Figure S5.** Hydrogels with different SA concentrations (a) Cumulative release quantity (b) Cumulative release percentage (c) Cumulative drug release rate of hydrogels with different pH (d)Effect of temperature on cumulative drug release behavior.



**Figure S6.** UV spectra of buffer solution (a) 1wt% SA gel (b) 1.5wt% SA gel (c) 2wt% SA gel

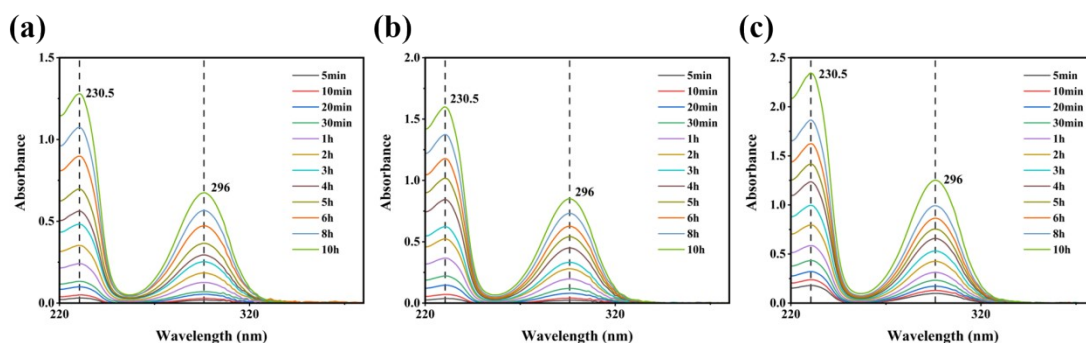


**Figure S7.** UV spectra of buffer solution (a) The pH of the hydrogel is 1.5 (b) The pH of the hydrogel is 2 (c) The pH of the hydrogel is 2.5

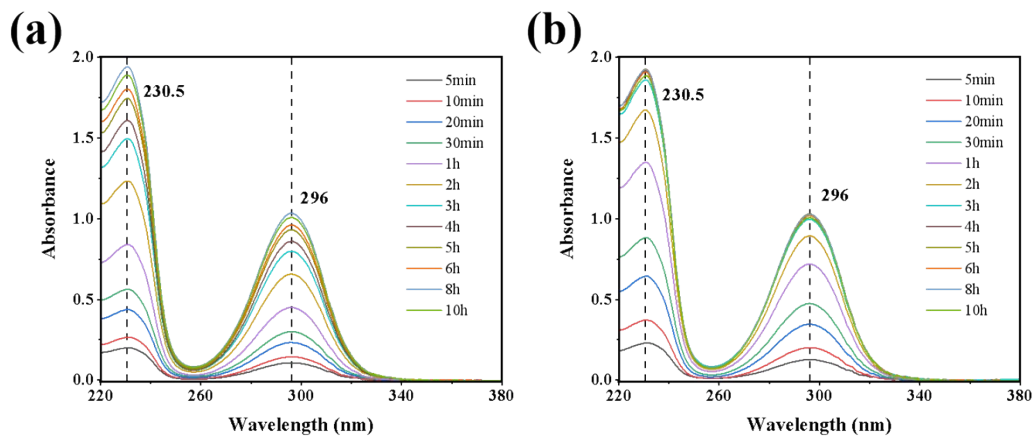


**Figure S8.** UV spectra of buffer solution (a) The ambient temperature is 37 °C (b) The ambient temperature is 50 °C

## 2.6 Factors influencing LGS/CTAB/SA hydrogel slow release

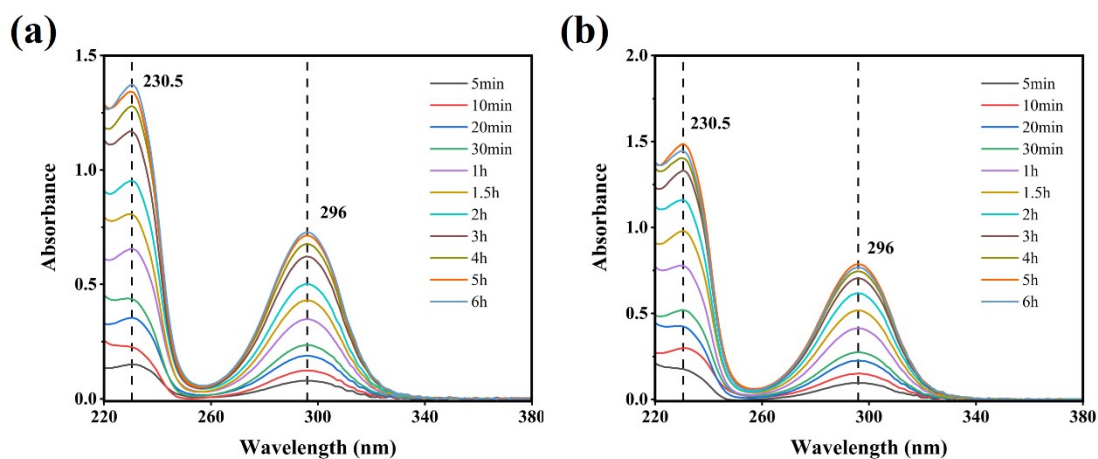


**Figure S9.** UV spectra of buffer solution (a) The ambient temperature is 37 °C (b) The ambient temperature is 50 °C

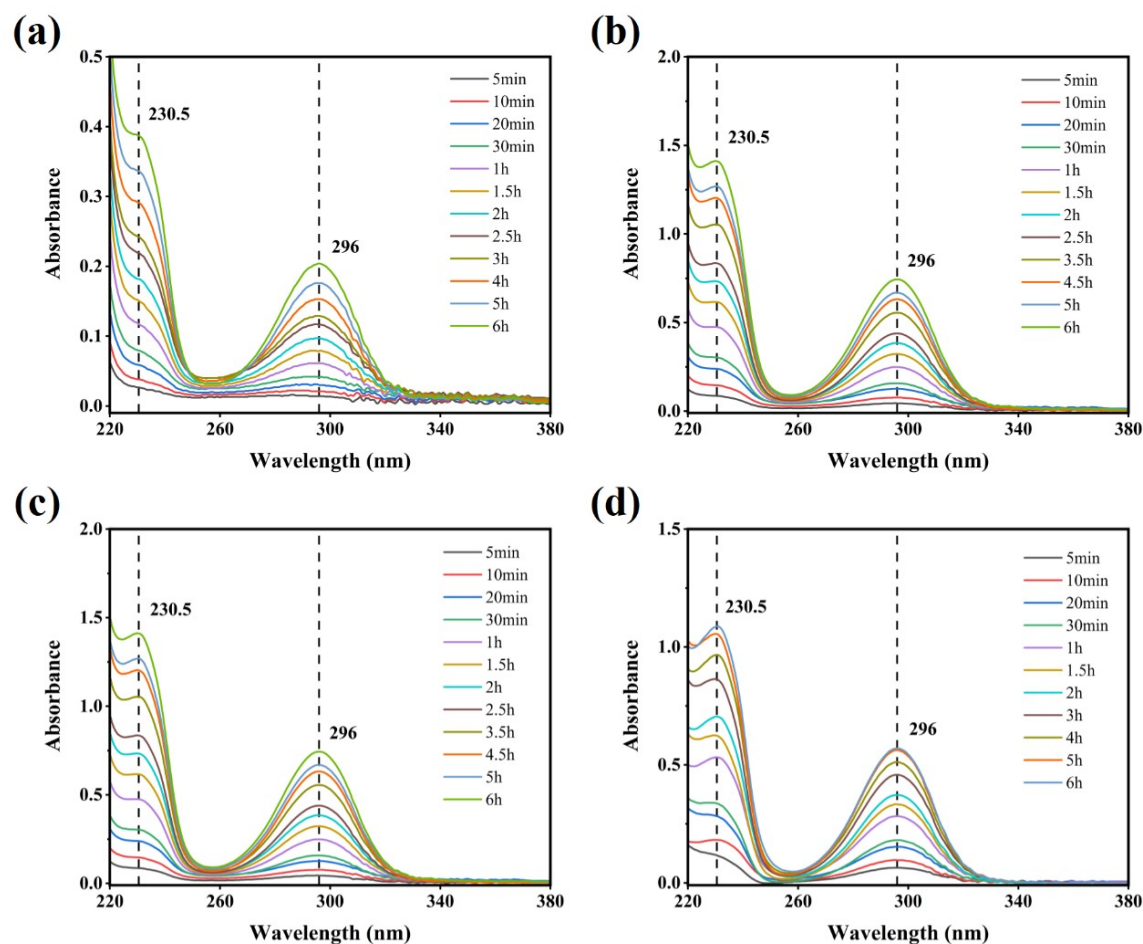


**Figure S10.** UV spectra of buffer solution (a) 0.1wt% SA gel (b) 0.3wt% SA gel (c) 0.5wt% SA gel (d) 1.0wt% SA gel

## 2.7 Physical modelling of drug release

To further investigate the effects of temperature and SA concentration on the slow-release behavior of LGS/CTAB/SA hydrogels, we continued to fit the drug release

profiles using Zero-order models (1.1)<sup>[1]</sup>, First-order models (1.2)<sup>[2]</sup>, Higuchi models (1.3)<sup>[3]</sup>, and Ritger-Peppas models (1.4)<sup>[4]</sup>. Among these models, the Ritger-Peppas model provided the best fit, with R<sup>2</sup> values above 0.96 (Table S2 and 3). In the Ritger-Peppas fitting model, a diffusion index  $n \leq 0.5$  is consistent with the Fickian diffusion release mechanism, while  $0.5 < n < 1$  indicates anomalous transport, which results from the combined effect of diffusion and dissolution.

$$\frac{M_t}{M_\infty} = K_0 t \quad (1.1)$$

$$\ln \left(1 - \frac{M_t}{M_\infty}\right) = -K_1 t \quad (1.2)$$

$$\frac{M_t}{M_\infty} = K_h t^{0.5} \quad (1.3)$$

$$\frac{M_t}{M_\infty} = K_r t^n \quad (1.4)$$

Where  $M_t$  is the cumulative concentration of SA released at time  $t$ ,  $K_0$ ,  $K_1$ ,  $K_h$ ,  $K_r$  are kinetic constants, and  $n$  is the diffusion index associated with the SA release mechanism.

**Table S2.** Parameters of drug release modelling at different temperatures

Samples	Zero-order	First-order			Higuchi		Ritger-Peppas		
Condition	R <sup>2</sup>	C <sub>0</sub>	K <sub>1</sub>	R <sup>2</sup>	K <sub>h</sub>	R <sup>2</sup>	K <sub>r</sub>	n	R <sup>2</sup>
25°C	0.8931	44.51	0.71	0.9591	19.07	0.9865	22.12	0.44	0.9918
37°C	0.8735	58.97	0.70	0.9746	25.51	0.9778	28.95	0.44	0.9836
50°C	0.8080	61.04	0.79	0.9591	27.30	0.9449	34.26	0.40	0.9613

**Table S3.** Parameters of drug release modelling at different concentrations

Samples	Zero-order	First-order			Higuchi		Ritger-Peppas		
Condition	R <sup>2</sup>	C <sub>0</sub>	K <sub>1</sub>	R <sup>2</sup>	K <sub>h</sub>	R <sup>2</sup>	K <sub>r</sub>	n	R <sup>2</sup>
0.1wt%	0.9791	25.86	0.37	0.9386	9.7514	0.9981	9.1343	0.5386	0.9933
0.3wt%	0.9662	29.73	0.35	0.9817	11.7246	0.9981	9.6229	0.5854	0.9996
0.5wt%	0.9274	35.72	0.47	0.9800	15.3389	0.9968	14.0213	0.5299	0.9949
1wt%	0.8931	44.51	0.71	0.9591	19.0716	0.9865	22.1185	0.4353	0.9918

## References

- [1] Ilgin P, Ozay H, Ozay O. A new dual stimuli responsive hydrogel: Modeling approaches for the prediction of drug loading and release profile [J]. *European Polymer Journal*, 2019, 113: 244-53.
- [2] Zhu W, Long J, Shi M. Release Kinetics Model Fitting of Drugs with Different Structures from Viscose Fabric [J]. *Materials*, 2023, 16(8).
- [3] Higuchi T. MECHANISM OF SUSTAINED-ACTION MEDICATION. THEORETICAL ANALYSIS OF RATE OF RELEASE OF SOLID DRUGS DISPERSED IN SOLID MATRICES [J]. *Journal of pharmaceutical sciences*, 1963, 52: 1145-9.
- [4] Peppas N A. 1. Commentary on an exponential model for the analysis of drug delivery: Original research article: a simple equation for description of solute release: I II. Fickian and non-Fickian release from non-swelling devices in the form of slabs, spheres, cylinders or discs, 1987 [J]. *Journal of controlled release : official journal of the Controlled Release Society*, 2014, 190: 31-2.